Superhard Monoborides: Hardness Enhancement through Alloying in $W_{1-x}Ta_xB$

Michael T. Yeung, Jialin Lei, Reza Mohammadi, Christopher L. Turner, Yue Wang, Sarah H. Tolbert, and Richard B. Kaner**

Superhard metals possess many benefits over traditional superhard materials such as diamond and cubic boron nitride. Most notably, they are easy to synthesize. They can be made at ambient pressure and thus can be cast from the melt like common metals. Furthermore, their metallic character allows them to be easily cut and shaped post-synthesis by electric discharge machining. The scientific factors involved in designing mechanically superhard compounds (Vickers hardness, $H_v \geq 40$ GPa) are complex: both elastic deformations (reflected in bulk modulus and shear resistance) and plastic deformations (reflected in elastic limits) must be optimized. Due to limitations in our ability to control material strength, the design of superhard materials is quite difficult. As such, there are only a handful of material compositions in existence known to be intrinsically superhard: diamond, cubic boron nitride, rhenium diboride, tungsten tetraboride, and chromium tetraboride.[1–4]

In 2005, we suggested that superhard compounds can be designed rather than discovered by following two simple rules.[5] The first step is to start with a high valence electron density, which leads to a large bulk modulus and high incompressibility.[1] The second step is to add short, strong covalent bonds to prevent shear and slipping of planes. For example, diamond is both the hardest and stiffest single-phase material known with a hardness of 70–110 GPa, a bulk modulus of 442 GPa, and a valence electron density of 0.71 e^- $Å^{-3}$.[6] These design rules can be applied to yield superhard metals by introducing short, highly covalent bonds using electron deficient atoms such as boron into metals with a large number of valence electrons, such as rhenium and tungsten.[4,7,8] Based on these ideas, it is not surprising that the five aforementioned superhard compositions are either fully covalent compounds, or they are the highest boride in a metal boride system.[9] In the case of the heavy metal tungsten, the simplest method to obtain a superhard phase is by introducing at least four molar equivalents of boron to yield WB_4. This increases the covalent bonding, and resulted in the first superhard composition in the tungsten–boron system.[8]

With the lower borides of tungsten, the significantly reduced level of covalent bonding should result in softer materials. Pristine tungsten tetraboride, the highest boride in the W–B system, is superhard with a Vickers hardness of ≈43 GPa under a load of 0.49 N. As such, tungsten monoboride (WB) should be significantly softer.[8] Experimental hardness measurements confirm that pristine WB is not naturally superhard, exhibiting a Vickers hardness of 36 GPa under a load of 0.49 N.[10] More rigorous computational studies have shown that WB should have a high shear modulus, but not nearly as high as those found in superhard materials.[11,12] Furthermore, in tungsten monoboride, the tungsten–tungsten bond distance (2.8 Å) approaches that of pure tungsten metal (2.7 Å), which suggests significantly stronger metallic bonding character. This brings with it some of the malleability and toughness found in conventional metals. Indeed, WB is suggested to have a good balance between hardness and ductility, which can lead to higher wear resistance.[13]

Because of the higher metallic character, metallic bonding should play a greater role in the mechanical properties of tungsten monoboride. Unfortunately, metallic bonding is generally weak. Metals, while possessing high electron density and incompressibility, have nondirectional metallic bonds,[9] which allows for transient bond breaking and dislocation formation. This is why most metals are ductile and malleable.[9] Based on our design rules, the best way to increase the hardness of metallic tungsten monoboride would be to add more equivalents of boron to yield the more covalent tungsten tetraboride. For the lower borides, however, a different method must be employed.

Here, we demonstrate an alternative approach, where we identify the crystallographic planes that slip at the lowest loads, and from there, we can find ways to increase the mechanical strength of these planes to make tungsten monoboride superhard. This is accomplished by: i) identifying the weak slip plane and ii) selectively strengthening this plane through solid solution hardening. We have followed the aforementioned approach to create a completely new superhard material ($W_{0.5}Ta_{0.5}B$). This approach suggests that along with the previously discussed design rules of incompressibility and shear, bonding motifs can also play an important role in materials strength.

Tungsten monoboride crystallizes in either a low temperature tetragonal or a high temperature orthorhombic unit cell. The primary difference between these two phases is found in

M. T. Yeung, J. Lei, C. L. Turner, Dr. Y. Wang, Prof. S. H. Tolbert, Prof. R. B. Kaner
Department of Chemistry and Biochemistry and California NanoSystems Institute
University of California
Los Angeles, CA 90095, USA
E-mail: tolbert@chem.ucla.edu; kaner@chem.ucla.edu
Prof. R. Mohammadi
Department of Mechanical and Nuclear Engineering
Virginia Commonwealth University
Richmond, VA 23284, USA
Prof. S. H. Tolbert, Prof. R. B. Kaner
Department of Materials Science and Engineering and California NanoSystems Institute
University of California
Los Angeles, CA 90095, USA

DOI: 10.1002/adma.201601187

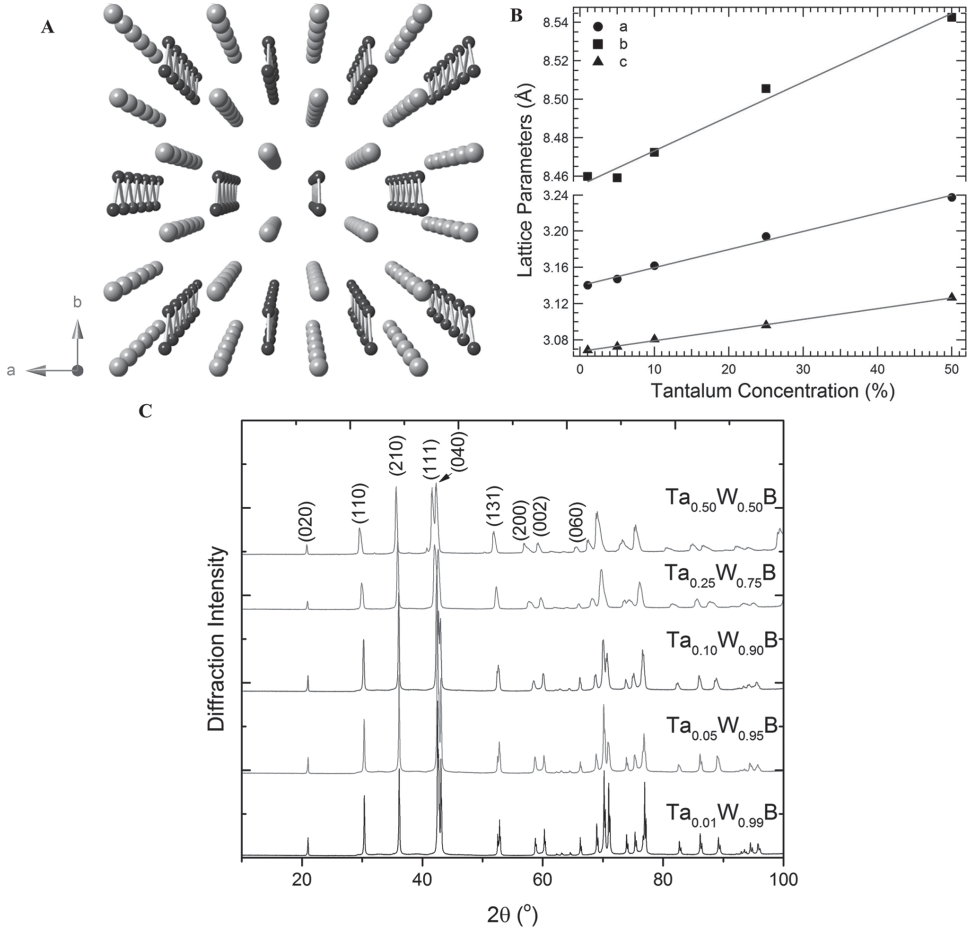

Figure 1. A) Crystal structure of high-temperature, orthorhombic tungsten monoboride, WB. Tungsten atoms are gray. B) The *a*, *b*, and *c* lattice parameters of $Ta_xW_{1-x}B$ ($x = 0.01$, 0.05, 0.10, 0.25, and 0.50). Note the linear progression of the lattice parameters with respect to tantalum content is consistent with Vegard's law. C) Powder X-ray diffraction patterns of $Ta_xW_{1-x}B$ ($x = 0.01$, 0.05, 0.10, 0.25, and 0.50) with peaks indexed to orthorhombic WB (JCPDS Card #00-006-0541).

the layer of boron chains, where in the tetragonal (low temperature) form, the boron chains alternate orthogonally, while in the orthorhombic (high temperature) form the boron chains are all aligned along the *a*-axis. Both structures possess a bilayer of tungsten atoms; the high temperature orthorhombic phase is shown in **Figure 1**A.

The bilayers of tungsten atoms separated by boron chains in WB are likely to dominate the mechanical properties of the material. Because tungsten monoboride (unlike tungsten tetraboride, WB_4) is a lower boride, the number of covalent bonds that can prevent the formation or movement of dislocations is limited. This fact, combined with the W–W bond lengths approaching that of tungsten metal, suggests that the hardness of WB is likely to be limited by slip in the tungsten bilayers. Indeed, computational studies of isostructural chromium monoboride have shown that the metal bilayer is indeed a slip plane.[17] As a result, if we can prevent dislocations in this metallic plane, we should be able to increase the overall hardness of tungsten monoboride.

Therefore, solid-solution strengthening has the potential to dramatically alter the mechanical properties of the WB system. Specifically, by substituting tungsten with larger atoms, slipping of the metallic planes can be reduced through dislocation pinning. With higher resistance to dislocations, the overall hardness should increase. As such, we chose to substitute tantalum onto the tungsten sites because tantalum has a similar valence, electronegativity, and only a modestly larger atomic radius when compared to tungsten. Furthermore, tantalum monoboride crystallizes into the same phase as the high temperature form of tungsten monoboride, which satisfies the Hume–Rothery rules for solid solutions. It should be noted that the end members of $W_{1-x}Ta_xB$ are not known to be superhard, and as such this is an excellent system to study.[18]

Tantalum monoboride crystallizes in an orthogonal unit cell, and when combined with the fast cooling rate of the copper hearth of the arc melter, it is expected that all $W_{1-x}Ta_xB$ compositions (where $x = 0.01$–0.5) will crystallize in the orthorhombic phase. Indeed, powder X-ray diffraction (XRD) suggests that even at 1% Ta concentration, as seen in $W_{0.99}Ta_{0.01}B$, the favored phase is the high temperature orthorhombic modification. Moreover, TaB is miscible in WB at high concentrations with no secondary phases as observed by powder X-ray diffraction (Figure 1C). There is a noticeable shift toward larger lattice

parameters with increased tantalum concentration, which is expected because tantalum (1.343 Å) has a slightly larger atomic radius when compared to tungsten (1.299 Å).[19] As seen in Figure 1B, these lattice parameters increase linearly, as expected from Vegard's law. This suggests a well-behaved alloy system with tantalum randomly distributed across the tungsten sites. Back-scattered scanning electron microscopy confirms that there are no secondary phases, and elemental mapping with electron dispersive spectroscopy (EDS) suggests that both tantalum and tungsten are well dispersed (Figure S1A, Supporting Information). Transmission electron microscopy of freshly fractured and crushed powder suggests that the samples are highly crystalline and not nanostructured, as seen in Figure S1B (Supporting Information). The lack of a secondary phase observed by XRD, EDS, and electron microscopy indicates that extrinsic hardening mechanisms such as precipitation hardening or dispersion hardening are not responsible for the observed mechanical properties.

Vickers hardness was then measured under loads of 0.49, 0.98, 1.96, 2.9, and 4.9 N (**Figure 2**). Under a low load of 0.49 N, the tungsten monoboride sample containing 1% tantalum has a Vickers hardness of ≈35.1 GPa, in good agreement with a previously reported value of 36 GPa for pristine, polycrystalline WB.[10] As the tantalum concentration is increased, there is an increase in hardness. This trend is linear with Ta concentration, reaching 42.8 GPa at the 50% composition. This breaks the threshold for superhard materials ($H_v \geq 40$ GPa); therefore, $W_{0.5}Ta_{0.5}B$ can be considered as a new superhard metal. Aside from WB_4, this is the only other superhard composition in the tungsten–boron system. And unlike WB_4, which is understood to derive its hardness purely from the covalent boron network, it appears that hardness in tungsten monoboride is achieved through a combination of covalent bonding and solution effects.

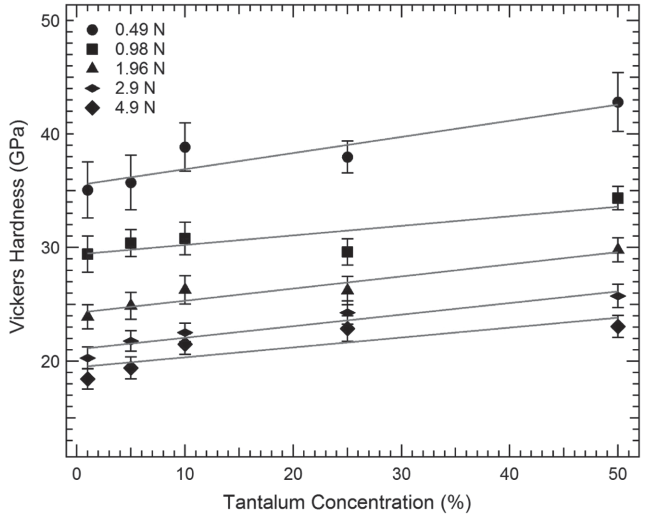

Figure 2. The Vickers indentation hardness of $Ta_xW_{1-x}B$ as a function of different loads (0.49 N per 50 gram-force $r^2 = 0.85$, 0.98 N per 100 gram-force $r^2 = 0.70$, 1.96 N per 200 gram-force $r^2 = 0.92$, 2.9 N per 300 gram-force $r^2 = 0.91$, and 4.9 N per 500 gram-force $r^2 = 0.71$) follows a linear trend. The hardness value of the 50 at% Ta composition under a load of 0.49 N is 42.8 ± 2.6 GPa indicating that $W_{0.5}Ta_{0.5}B$ is a superhard material.

This linear hardness trend that maximizes at a 50% concentration is quite unusual amongst the borides. For example, WB_4 forms solid solutions with tantalum, chromium, and manganese, but the hardness trend for WB_4 solid solutions is not linear.[2] For the WB_4 system, the highest hardness values are achieved at very low substitution levels (≈5 at%) and are believed to arise mostly from electronic structure effects.[8] Likewise, the hardness of $Os_{1-x}Ru_xB_2$ solid solutions is linear with composition, but it does not show any hardness maxima near 50% concentration. Instead, the data exhibit simple Vegard's law behavior connecting the two end members.[20] The unique behavior in $W_{1-x}Ta_xB$, combined with inspection of the orthorhombic crystal structure, suggests that modification of the metallic bilayer may be responsible for the increase in the material's strength. By substituting tungsten with larger tantalum atoms, plane slipping will be diminished through dislocation pinning. At 50% concentration, pinning should be maximized, and this is reflected in the hardness measurements. Indeed, $W_{0.5}Ta_{0.5}B$ is much harder than its parent structures: WB (36 GPa[10] at 0.49 N) and TaB (30.7 GPa[21] at 0.49 N). This chemical tuning of the structure shows that the hardness of tungsten monoboride can be increased through solid solution hardening.

To confirm the hardening effects of substituting tantalum into the metallic bilayer, high-pressure diffraction studies are used to correlate macroscopic hardness with microscopic deformations. By compressing samples under nonhydrostatic stress in a high-pressure diamond anvil cell, conditions similar to those found under the indenter tip can be controllably produced in a geometry that can be readily probed using X-ray diffraction. Such experiments can provide a lattice specific measure of yield strength and the predominant slip systems available in the material.[22] High-pressure radial diffraction is a well-known technique that has been satisfactorily used previously to determine the amount of load each plane supports in nanocrystalline WB.[23]

Here, high-pressure radial diffraction is used to determine which planes in tungsten monoboride limit the hardness. We can specifically learn about the slip system in the material by differential strain, which is given by the ratio of differential stress to shear modulus (t/G). Linearly increasing t/G values correspond to elastically supported differential strain, but when the curve plateaus, it corresponds to the onset of plastic deformation. Planes that have a low t/G plateau pressure tend to dislocate and slip easily, while planes that have a high t/G plateau pressure can support more deformation.[4] For $W_{0.50}Ta_{0.50}B$, the planes (200), (020), and (002) were chosen for study because they represent the anisotropy of the unit cell. Dislocations in the (200) set of planes cut between the boron–boron chains, while the (020) set of planes cut through the tungsten bilayer, and the (002) planes cut through the boron–boron bonds (Figure 1A). In other words, the (200) and (002) represents more covalent/boron bonding, while the (020) possesses more metallic/tungsten bonding.

As can be seen in **Figure 3**, the elastically supported differential strain for the (200) and (002) planes is lower than that of the (020) planes at lower pressures, suggesting that the bonds in the (200) and (002) directions are stiffer. As the pressure is increased, the (020) planes are also the first to plateau at

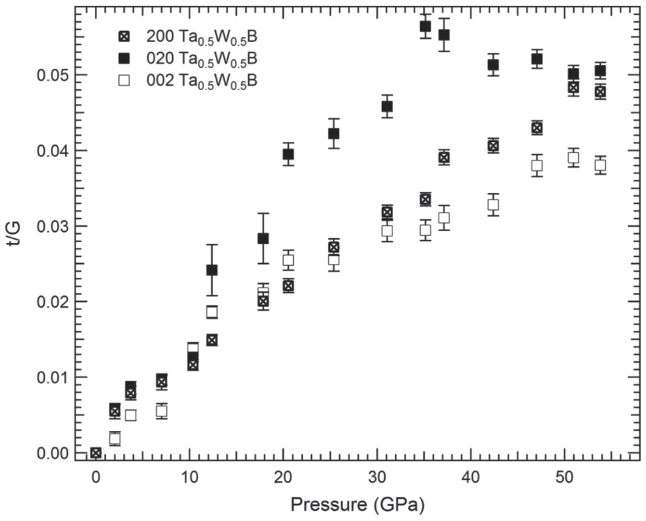

Figure 3. The differential strain plot of $W_{0.5}Ta_{0.5}B$ with respect to the (200), (020), and (002) sets of planes. The (020) planes support the highest differential strain (t/G) and indicate that they are the load-bearing planes.

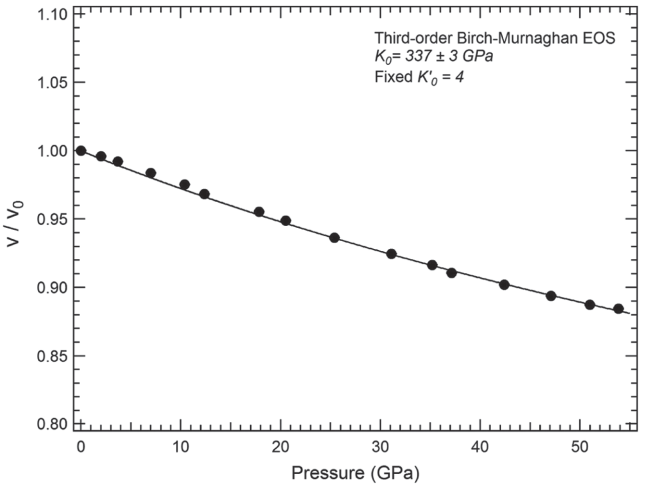

Figure 4. The deformation in the unit cell volume is fit to a third order Birch–Murnaghan equation of state, and shows that $W_{0.5}Ta_{0.5}B$ is ultraincompressible.

36 GPa. The plateau is an indication of transition from elastic to plastic deformation, and so these data indicate that the (020) planes constitute the primary slip system for this material, in agreement with calculations on isostructural CrB.[17] While these factors all suggest that the metal bilayers are the weakest directions in the material, the actual plateau value of 5.1% differential strain is quite high. We note that unlike differential stress, differential strain cannot be directly related to hardness because elastic anistropy can produce high strains in elastically soft directions. Unfortunately, the elastic constants for $W_{0.50}Ta_{0.50}B$ are not known, so the plateau value of the differential stress cannot be directly calculated from the plateau differential strain. Despite these issues, the (020) plateau strain value is high, and the fact that the (200) curve only meets the (020) curve near 50 GPa further indicates that substituting Ta into WB appears to be an effective way to strengthen the weakest lattice direction in $W_{0.50}Ta_{0.50}B$.

Intriguingly, the detailed behavior of the (020) set of planes further reveals insights into the nature of the bonding. As can be seen in Figure 3, the differential strain supported by the (020) planes increases up to a maxima of 5.5% differential strain at 35 GPa, and then the strain decreases. This nonmonotonic behavior is reminiscent of pure niobium metal.[15] These results thus further suggest that the tungsten bilayer, represented by the (020) planes, behaves like a pure metal. Thus, because this system combines metal–metal bonding and metal–boron bonding, hardness needs to be optimized using two methods. Where present, metal–boron bonds can prevent slip much like they do in WB_4. For the metal–metal bilayers, however, which are the first planes to slip, solid-solution effects are needed to reduce the slip.

From the high-pressure studies, the bulk modulus of $W_{0.5}Ta_{0.5}B$ was determined to be 337 ± 3 GPa using a second order Birch–Murnaghan equation-of-state (**Figure 4**). This demonstrates that $W_{0.5}Ta_{0.5}B$ is not only superhard, but also ultraincompressible. This value is slightly lower than the theoretically predicted bulk modulus of 350 GPa for WB, which is expected because tantalum contains fewer electrons than tungsten.[11,23] This tungsten monoboride solid solution is therefore even more incompressible than tungsten tetraboride (326 ± 3 GPa), the other superhard boride in the tungsten–boron system.[24] This was expected, since incompressibility is related to high electron density that comes from the tungsten. With a high tungsten content and tungsten–tungsten bonds that approach those found in tungsten metal, tungsten monoboride should have a high bulk modulus.

Oxidation resistance was measured using thermal gravimetric analysis. In practical applications, high oxidation resistance is needed because the act of machining generates high temperatures from friction. Oxidation of $W_{0.5}Ta_{0.5}B$ begins at 550 °C in air (Figure S2, Supporting Information). This suggests that $W_{0.5}Ta_{0.5}B$ has a higher resistance to oxygen than tungsten carbide, which begins oxidizing at 500 °C.[25] Tungsten carbide is one of the most useful materials for cutting tools.[26] The added oxidation resistance provided by adding tantalum, is likely due to the formation of a protective oxide coating, which prevents further oxidation until 550 °C.[27] Furthermore, tungsten monoboride behaves as a metallic conductor as seen with a temperature versus resistance plot (Figure S3, Supporting Information), which suggests that tungsten monoboride can easily be shaped post-synthesis via electric discharge machining.

The greatly increased role of metallic bonding in the hardness of WB offers an intriguing line of inquiry into superhard materials. Typically, nondirectional metallic bonds are prone to slip and thus, conventional wisdom would suggest that the best way to make a superhard metal would be to add more boron until covalent bonding dominates and prevents the movement of dislocations. As such, superhardness should generally be found in strongly covalent materials such as diamond or tungsten tetraboride, which are both brittle materials. Here, we demonstrate that metallic bilayers can be present in a superhard material if they are properly engineered to reduce the slip. Solid solution strengthening can be used to increase the hardness of tungsten monoboride because it is effective at

strengthening these metal bilayers. Furthermore, high-pressure radial diffraction experiments confirm that the metallic bilayer of tungsten monoboride is the easy slip system of the material and should be the focus of solid-solution optimization. In conclusion, strengthening of the weakest planes is an alternate and viable approach to creating new superhard materials in more metallic materials.

Experimental Section

Tungsten (Strem, 99.95%), tantalum (Roc/Ric, 99.9%), and boron (Materion, 99%) powders were stoichiometrically ground in an agate mortar and pestle (typical total loadings were 1 g). Some samples had a slight excess of boron due to boron sublimation from the high temperatures of arcing. The homogeneous powders were pressed into a pellet, arced, turned over, and re-arced to ensure homogeneity. Samples were arced under high-purity argon under ambient pressure. The ingots were then bisected, with one half crushed for powder X-ray diffraction, high-pressure radial diffraction, and thermal gravimetric analysis. The other half was mounted in epoxy and polished, for hardness and scanning electron microscopy (SEM), and for phase analysis. Mounted samples were polished with a SouthBay Technologies Polishing Station using polishing papers from 120 to 1200 grit (Allied High Tech Products Inc.).

Samples were analyzed by powder X-ray diffraction on a Panalytical X'Pert diffractometer using a Cu $K_{\alpha 1}$ source (λ = 1.5418 Å). The as-collected spectra were compared against JCPDS Card #00-006-0541 using X'Pert HighScore Plus as the processing software. Powder samples were then refined by size using a solvent suspension method, and imaged under a TF-20 transmission electron microscope (TEM) for size analysis. Size-refined powders were then used for high pressure radial diffraction.

Polished samples were imaged under backscatter SEM using a Nova 230 electron microscope with EDS used to determine homogeneity. Polished samples were measured for hardness on a Micromet 2103 equipped with a pyramid diamond indenter tip. With a dwell time of 15 s, the samples were indented under loads of 0.49, 0.98, 1.96, 2.9, and 4.9 N. Indent diagonals were measured using a Zeiss Axiotech 100HD optical microscope (Carl Zeiss Vision GmbH, Germany). Vickers hardness was determined from Equation (1) using the arithmetic mean of 14 randomly chosen indents:

$$H_v = \frac{1854.4\,P}{d^2} \tag{1}$$

where P is the applied load and d is the average of the diagonals.

Radial diffraction was performed at the Advanced Light Source at Lawrence Berkeley National Labs using a diamond anvil cell. Incompressibility was determined using the third-order finite strain Birch–Murnaghan equation of state (Equation (2)):

$$P = \frac{3}{2}K_0\left[\left(\frac{V}{V_0}\right)^{-\frac{7}{3}} - \left(\frac{V}{V_0}\right)^{-\frac{5}{3}}\right]\left\{1 - \frac{3}{4}(4-K)\left[\left(\left(\frac{V}{V_0}\right)^{-\frac{2}{3}} - 1\right)\right]\right\} \tag{2}$$

where P is the applied load, K_0 is the bulk modulus, V is the deformed unit cell volume, V_0 is the undeformed unit cell volume, and K_0' is the derivative of the K_0 with respect to P. Here, K_0' is fixed to 4.

Differential strain was interpreted using lattice strain theory from the high-pressure radial diffraction using Equation (3):[14]

$$d_{meas}(hkl) = d_{hydro}(hkl)\,[1 + (1 - 3\cos^2\Psi)]\,Q(hkl) \tag{3}$$

where Ψ is the angle between the diffracting plane normal and the maximum stress axis, $d_{hydro}(hkl)$ is the hydrostatic d-spacing (measured when Ψ = 54.7°), and $d_{meas}(hkl)$ is the measured d-spacing under pressure. $Q(hkl)$, the orientation dependent differential strain, can be written as:

$$\frac{t(hkl)}{G} = 6\,Q(hkl) \tag{4}$$

where G is the aggregate shear strain, and t is the differential stress.[15] The differential stress, t, can be rewritten using the Tresca yield criterion:

$$t = \sigma_{axial,\,max} - \sigma_{radial,\,min} \leq 2\tau = \sigma_y \tag{5}$$

where $\sigma_{axial,\,max}$ is the maximum stress along the axial direction, $\sigma_{radial,\,min}$ is the minimum stress along the radial direction, and σ_y is the yield strength.[16] The elastically supported differential stress, t, enables one to estimate the lower bound of the material's yield strength, σ_y.

Thermal stability in air of each of the materials was determined using a Pyris Diamond thermogravimetric/differential thermal analyzer. Powder samples were heated in air up to 200 °C at a rate of 20 °C min^{-1}, held for 20 min to remove residual moisture, and then heated up to 1000 °C at a rate of 2 °C min^{-1}.

Supporting Information

Supporting Information is available from the Wiley Online Library or from the author.

Acknowledgements

The authors would like to thank Prof. Benjamin M. Wu at the UCLA Department of Bioengineering for use of his micro-indentation system. Financial support for this research came from the National Science Foundation under grant DMR-1506860 Solid State and Materials Chemistry Program in the Division of Materials Research (R.B.K. and S.H.T.) and a National Science Foundation-IGERT- Materials Creation Training Program DGE-0654431 Fellowship (M.T.Y.). Portions of this work were performed at the Advanced Light Source, Lawrence Berkeley National Laboratory. The Advanced Light Source was supported by the Director, Office of Science, Office of Basic Energy Sciences, of the U.S. Department of Energy under Contract No. DE-AC02-05CH11231.

Received: March 1, 2016
Revised: March 25, 2016
Published online: May 20, 2016

[1] V. V. Brazhkin, A. G. Lyapin, R. J. Hemley, *Philos. Mag. A* **2002**, *82*, 231.
[2] R. Mohammadi, M. Xie, A. T. Lech, C. L. Turner, A. Kavner, S. H. Tolbert, R. B. Kaner, *J. Am. Chem. Soc.* **2012**, *134*, 20660.
[3] a) K. Kotmool, T. Kaewmaraya, S. Chakraborty, J. Anversa, T. Bovornratanaraks, W. Luo, H. Gou, P. C. Piquini, T. W. Kang, H.-k. Mao, R. Ahuja, *Proc. Natl. Acad. Sci. USA* **2014**, *111*, 17050; b) R. Mohammadi, R. B. Kaner, in *Encyclopedia of Inorganic and Bioinorganic Chemistry* **2012**, 1; c) A. Knappschneider, C. Litterscheid, D. Dzivenko, J. A. Kurzman, R. Seshadri, N. Wagner, J. Beck, R. Riedel, B. Albert, *Inorg. Chem.* **2013**, *52*, 540.
[4] H.-Y. Chung, M. B. Weinberger, J. B. Levine, A. Kavner, J.-M. Yang, S. H. Tolbert, R. B. Kaner, *Science* **2007**, *316*, 436.
[5] R. B. Kaner, J. J. Gilman, S. H. Tolbert, *Science* **2005**, *308*, 1268.
[6] I. Aleksandrov, A. Goncharov, A. Zisman, S. Stishov, Zh. Eksp. *Teor. Fiz.* **1987**, *93*, 691.
[7] R. W. Cumberland, M. B. Weinberger, J. J. Gilman, S. M. Clark, S. H. Tolbert, R. B. Kaner, *J. Am. Chem. Soc.* **2005**, *127*, 7264.

[8] R. Mohammadi, A. T. Lech, M. Xie, B. E. Weaver, M. T. Yeung, S. H. Tolbert, R. B. Kaner, *Proc. Natl. Acad. Sci. USA* **2011**, *108*, 10958.
[9] Q. Gu, G. Krauss, W. Steurer, *Adv. Mater.* **2008**, *20*, 3620.
[10] G. Samsonov, *Dokl. Akad. Nauk SSSR* **1957**, *113*, 1299.
[11] H.-H. Chen, Y. Bi, Y. Cheng, G. Ji, F. Peng, Y.-F. Hu, *Phys. B: Condens. Matter* **2012**, *407*, 4760.
[12] X. Xu, K. Fu, L. Li, Z. Lu, X. Zhang, Y. Fan, J. Lin, G. Liu, H. Luo, C. Tang, *Phys. B: Condens. Matter* **2013**, *419*, 105.
[13] H. Engqvist, S. Ederyd, N. Axén, S. Hogmark, *Wear* **1999**, *230*, 165.
[14] a) A. K. Singh, *J. Appl. Phys.* **1993**, *73*, 4278; b) A. K. Singh, C. Balasingh, H.-k. Mao, R. J. Hemley, J. Shu, *J. Appl. Phys.* **1998**, *83*, 7567.
[15] A. K. Singh, H.-P. Liermann, *J. Appl. Phys.* **2011**, *109*, 113539.
[16] A. L. Ruoff, *J. Appl. Phys.* **1975**, *46*, 1389.
[17] L. Han, S. Wang, J. Zhu, S. Han, W. Li, B. Chen, X. Wang, X. Yu, B. Liu, R. Zhang, Y. Long, J. Cheng, J. Zhang, Y. Zhao, C. Jin, *Appl. Phys. Lett.* **2015**, *106*, 221902.
[18] a) S. Okada, K. Kudou, I. Higashi, T. Lundström, *J. Cryst. Growth* **1993**, *128*, 1120; b) S. Okada, K. Kukou, T. Lundström, *Jpn. J. Appl. Phys.* **1995**, *34*, 226.
[19] L. Pauling, *J. Am. Chem. Soc.* **1947**, *69*, 542.
[20] M. B. Weinberger, J. B. Levine, H.-Y. Chung, R. W. Cumberland, H. I. Rasool, J.-M. Yang, R. B. Kaner, S. H. Tolbert, *Chem. Mater.* **2009**, *21*, 1915.
[21] A. Ivankov, *Handbook of Hardness Data*, Naukova Dumka, Kiev **1968**.
[22] R. J. Hemley, H.-k. Mao, G. Shen, J. Badro, P. Gillet, M. D. Häusermann, *Science* **1997**, *276*, 1242.
[23] H. Dong, S. M. Dorfman, Y. Chen, H. Wang, J. Wang, J. Qin, D. He, T. S. Duffy, *J. Appl. Phys.* **2012**, *111*, 123514.
[24] M. Xie, R. Mohammadi, Z. Mao, M. M. Armentrout, A. Kavner, R. B. Kaner, S. H. Tolbert, *Phys. Rev. B* **2012**, *85*, 064118.
[25] R. F. Voitovich, É. A. Pugach, *Powder Metall. Met. Ceram.* **1973**, *12*, 314.
[26] a) K. A. Brookes, *Met. Powder Rep.* **1995**, *50*, 22; b) H. E. Exner, *Int. Met. Rev.* **1979**, *24*, 149.
[27] X. Zhang, G. E. Hilmas, W. G. Fahrenholtz, *J. Am. Ceram. Soc.* **2008**, *91*, 4129.